Climate Dynamics
https://doi.org/10.1007/s00382-021-05857-y

Influence of Tibetan Plateau on the North American summer monsoon precipitation

Qin Wen[1,2,8,9] · Zixuan Han[3] · Haijun Yang[4] · Jianbo Cheng[5] · Zhengyu Liu[6] · Jian Liu[1,2,7]

Received: 21 February 2021 / Accepted: 17 June 2021

Abstract
It has been well known that the uplift of the Tibetan Plateau (TP) can significantly enhance the Asian monsoon. Here, by comparing the sensitivity experiments with and without the TP, we find that the TP uplift can also increase the precipitation of the North American Summer Monsoon (NASM), with atmosphere teleconnection accounting for 6% and oceanic dynamical process accounting for another 6%. Physically, the TP uplift generates a stationary Rossby wave train traveling from the Asian continent to the North Atlantic region, resulting in an high-pressure anomaly over the tropical-subtropical North Atlantic. This high pressure system enhances the low-level easterly winds, forcing an enhanced upward motion over the North American monsoon (NAM) region and then an increase in summer precipitation there. In addition, the TP uplift enhances the Atlantic meridional overturning circulation, which reduces the meridional temperature gradient and leads to a northward shift of Hadley Cell over eastern Pacific-Atlantic section. The latter shifts the convection center northward to 10°N and further increases the NASM precipitation. The enhanced NASM precipitation can also be understood by the northward shift of Intertropical Convergence Zone. Our study implies that the changes of NAM climate can be affected by not only local process but also remote forcing, including those from Asian highland region.

Keywords Tibetan Plateau · North American summer monsoon · Hadley circulation · Atlantic meridional overturning circulation · Intertropical convergence zone

1 Introduction

The Tibetan Plateau (TP), with an average elevation of more than 4000 m above sea level and a total area of 2.3 million square kilometers, is one of the most prominent features on Earth. The uplift of the TP has been known to generate a great impact on regional climate change, especially on Asian monsoon climate (Harrison et al. 1992; An 2001; Molnar et al. 2010). Until now, the TP uplift on Asian monsoon precipitation has been studied both by observations and model simulations. In observational studies, the documentation of planktonic foraminifer over the Arabian Sea indicates

✉ Qin Wen
wenq@pku.edu.cn

1 School of Geography, Nanjing Normal University, Nanjing 210023, China

2 Pilot National Laboratory for Marine Science and Technology (Qingdao), Open Studio for Ocean-Climate-Isotope Modeling, Qingdao 266100, China

3 College of Oceanography, Hohai University, Nanjing 210024, China

4 Department of Atmospheric and Oceanic Sciences, Institute of Atmospheric Science and CMA-FDU Joint Laboratory of Marine Meteorology, Fudan University, Shanghai 200438, China

5 School of Environmental Science and Engineering, Yancheng Institute of Technology, Yancheng 224051, China

6 Department of Geography, Ohio State University, Columbus, OH, USA

7 Jiangsu Provincial Key Laboratory for Numerical Simulation of Large Scale Complex Systems, School of Mathematical Science, Nanjing Normal University, Nanjing 210023, China

8 Key Laboratory of Virtual Geographic Environment (Nanjing Normal University), Ministry of Education, Nanjing 210023, China

9 Jiangsu Center for Collaborative Innovation in Geographical Information Resource Development and Application, Nanjing 210023, China

Published online: 28 June 2021

enhanced southwesterly winds and a strengthening of the Indian summer monsoon (Kroon et al. 1991; Prell et al. 1992). The aeolian "Red Clay" sediments over the Chinese Loess plateau suggest an onset of aeolian dust accumulation (An et al. 2001). The oxygen isotope composition of soil carbonates indicates changes in vegetation from forests to grasses in Pakistan (Quade et al. 1989), as well as a change from mixed needle-leaf or broad-leaf forests to grassland vegetation along the northeastern margin of the TP (Cerling et al. 1997). These widely distributed observations can be interpreted as signalling an environmental response to the TP uplift about 9–8 Myr ago (An et al. 2001). In model simulations, several studies investigate the Asian summer monsoon behavior under the TP elevation forcing (Boos and Kuang 2010; Park et al. 2012; Wu et al. 2012). Major results are that the uplift of the TP significantly increases the Asian monsoon intensity (Prell and Kutzbach 1992) and variability (Fallah et al. 2016). Considering different stages of TP uplift, the East Asian summer monsoon system similar to that of the present initially exists when the TP uplift 60% of its modern height and is gradually intensified with the continued plateau uplift (Jiang et al. 2008; Liu and Yin 2002; An et al. 2001). In addition, the uplift of different parts of the TP on distinct Asian monsoon climate has also been verified by recent numerical experiments (Zhang et al. 2010; Boos and Kuang 2010; Wu et al. 2012; Tang et al. 2013; Chen and Bordoni 2014).

However, few studies have focused on the impact of the TP topography on North American monsoon (NAM) climate. The NAM is one of the most complex and interesting atmospheric circulation features over the North America. Dominated by perennially dry conditions, the NAM contributes approximately 40 and 70% of the annual total precipitation for the southwest Unite States and northwest Mexico, respectively (Higgins et al. 1997; Adams and Comrie 1997). Paleo-climate research using fossil flowers to reconstruct Miocene climate over south Mexico shows that the environmental conditions of the Chiapas is warmer and drier during Miocene when the TP is not uplifted (Hernández et al. 2020). That is to say, the TP uplift is responsible for the wetter conditions over south Mexico in the present. However, the mechanisms are still unclear. The role of the TP on the NAM precipitation deserves an in-depth investigation, which is our focus in this study.

The drier conditions over NAM region during Miocene when the TP is not uplifted resembles the weakened NAM precipitation under global warming. The redistribution of NAM precipitation to global warming is usually conjectured to arise from two factors. One factor is the convection barrier related to the surface evapotranspiration and the tropospheric stability induced by greenhouse gas while the other is the moisture convergence related to monsoon circulation (Cook et al. 2013; Pascale et al. 2017). All these factors are related to atmospheric circulation and surface temperature. Previous works that study the NAM precipitation under global warming usually highlight the contributions from local regions, i.e., the Pacific and North Atlantic. For example, the sea surface temperature (SST) cooling in the North Atlantic can substantially alter the North Atlantic subtropical high, which may ultimately influence the NAM (Kushnir et al. 2010; Parsons et al. 2014; Wang et al. 2014). The NAM is also closely linked to tropical Pacific SST (Castro et al. 2001). The positive temperature anomaly over eastern-central Pacific can displace the North Pacific intertropical convergence zone and the South Pacific convergence zone equatorward, thereby directly reducing the NAM rainfall (Webster et al. 1998; Wang et al. 2012). However, the impacts from remote area, i.e., the Asian highland regions on the NAM climate have never been studied before. Our previous works suggest that the TP uplift may trigger a La Niña-like SST response over the tropical Pacific Ocean and an establishment of the Atlantic meridional overturning circulation (AMOC) (Wen and Yang 2020; Yang and Wen 2020). Building on these prior works, the TP uplift should be important for NAM climate change. How would the North American summer monsoon (NASM) precipitation response under the TP uplift? What is the role of the atmosphere and ocean? These questions have rarely been addressed in previous works. It is worth noting that the TP is reported to have experienced a faster warming than other regions in the Northern Hemisphere during past several decades (Duan et al. 2006) and will continue to warm more seriously in the future (Hu et al. 2015; Zhang et al. 2015). The TP uplift in our study includes the TP thermal forcing. The teleconnection between TP uplift and NAM precipitation in this study to some extent can be used to infer the future NAM change.

This paper is arranged as follows. An introduction to the model and experiments, as well as the methods is given in Sect. 2. Changes in NASM precipitation are illustrated in Sect. 3. Mechanisms for NASM precipitation change are analyzed in Sect. 4. Summary and discussion are given in Sect. 5.

2 Model and methods

2.1 Model and experiments

The Community Earth System Model (CESM1.0) is applied in this study. This model has been widely used to study the Earth's past, present, and future climate states (http://www2.cesm.ucar.edu/). CESM was developed by the U.S. National Centre for Atmospheric Research (NCAR) and is composed of an atmosphere model (Community Atmosphere Model; CAM5), ocean model (Parallel Ocean Program; POP2), land surface model (Community Land Model; CLM4), sea ice

model (Community Ice Code; CICE4) and one coupler (Wen and Yang 2020). The model grid employed in this study is T31_gx3v7. The CAM5 has 26 vertical levels, with the finite-volume nominal 3.75° × 3.75° grid. The CLM4 has the same horizontal resolution as the CAM5. The POP2 has 60 vertical levels and a uniform 3.6° spacing in the zonal direction. In the meridional direction, the grid is nonuniformly spaced: It is 0.6° near the equator, gradually increasing to the maximum 3.4° at 35°N/S and then decreasing poleward. The CICE4 has the same horizontal grid as the POP2. No flux adjustments are used in CESM1.0.

To fully assess the TP uplift on NASM precipitation, we separate the atmospheric and oceanic dynamical process by conducting two groups of simulations. The first set of simulations are performed using fully coupled (CPL) runs, including a 2400-year simulation with no modifications made to topography which we will refer to as "CTRL" and a 400-year no-mountain run called "NoTP". In CTRL, the model geometry, topography, and continents are realistic (Fig. 1a). The CTRL run reaches equilibrium state around 2000 years (Yang et al. 2015). The NoTP simulation starts from the year 2001 of CTRL, and is integrated for 400 years with the topography around the TP set to 50 m above the sea level (Fig. 1b). Except the topography elevation, all other boundary conditions, such as vegetation and albedo remain unmodified and they are free adjusted. The second set of simulations considers a slab ocean model (SOM), in which the ocean dynamical process has been shut-down and replaced by a mixed layer from the climatology of CTRL simulation. Two experiments in this group are named "CTRL_SOM" and "NoTP_SOM", in which the topography is set as that of "CTRL" and "NoTP", respectively. "CTRL_SOM"is integrated for 400 years and "NoTP_SOM" starts from the year 201 of "CTRL_SOM" and is integrated for 200 years. The equilibrium stages are deduced by using data from the last 50 years of integrations in SOM runs and last 100 years in CPL runs (outlined by light blue shadings in Fig. 2b, c). The difference between the "CTRL" and "NoTP" is for the sum of atmospheric and oceanic dynamical processes, and the difference between the "CTRL_SOM" and "NoTP_SOM" can be treated as atmospheric effect.

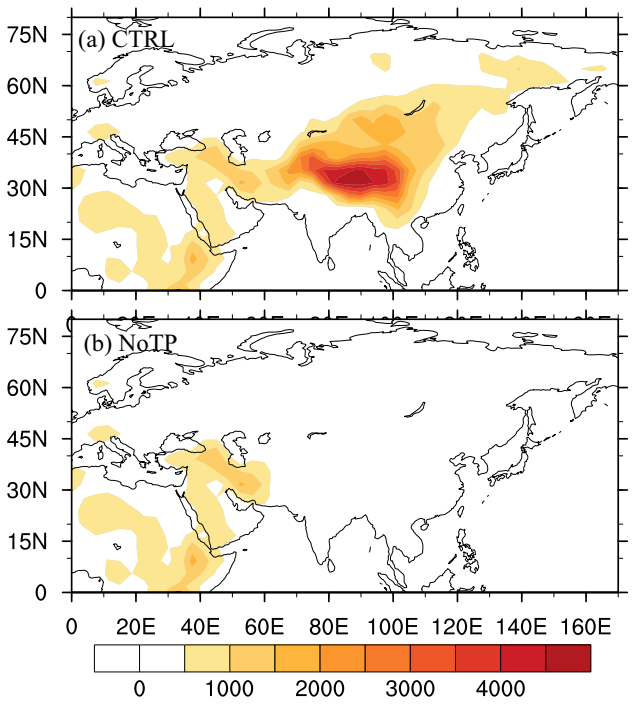

Fig. 1 Topography configuration (units: m) for **a** CTRL and **b** NoTP

2.2 North American monsoon region

According to Wang and Ding (2008), the NAM domain is delineated by the region in which the local summer precipitation minus local winter precipitation exceeding 2 mm/day and the local summer precipitation exceeds 55% of annual rainfall. Based on this definition, the global monsoon regions are clearly shown in Fig. 2a by using the GPCP data (outlined by purple contours) and our CTRL simulation (outlined by black contours). It is clearly shown that our CTRL simulation can well capture the spatial pattern of global monsoon domains, which is consistent with the findings of Liu et al (2016). Note that the NAM domain obtained in this study is primarily based on precipitation contrast in the solstice seasons and is larger than that traditionally recognized by many scientists working on the NAM (Wang et al. 2021). The NASM precipitation can be obtained by the weighted-area average local summer precipitation over the NAM area.

2.3 Moisture budget

To reveal the mechanisms that govern changes in NASM precipitation related to the TP uplift, we analyse changes in the moisture budget according to Chou et al. (2009):

$$P' = E' - \bar{\omega}\frac{\partial q'}{\partial p} - \omega'\frac{\partial \bar{q}}{\partial p} - \langle \bar{v} \bullet \nabla q' \rangle - \langle V' \bullet \nabla \bar{q} \rangle + R \qquad (1)$$

Here, P is precipitation, E is surface evaporation, ω is vertical velocity, q is specific humidity, p is pressure, V is horizontal wind vector, R is residual. Overbars represent monthly means in CTRL, and primes denote the difference between CTRL and NoTP. Based on this equation, the monsoon precipitation change can be decomposed into evaporation change (E'), the thermodynamic and dynamic changes of vertical moisture advection ($-\bar{\omega}\frac{\partial q'}{\partial p}$ and $-\omega'\frac{\partial \bar{q}}{\partial p}$), and thermodynamic and dynamic changes of horizontal moisture advection ($-\langle \bar{v} \bullet \nabla q' \rangle$ and $-\langle V' \bullet \nabla \bar{q} \rangle$) and the residual R.

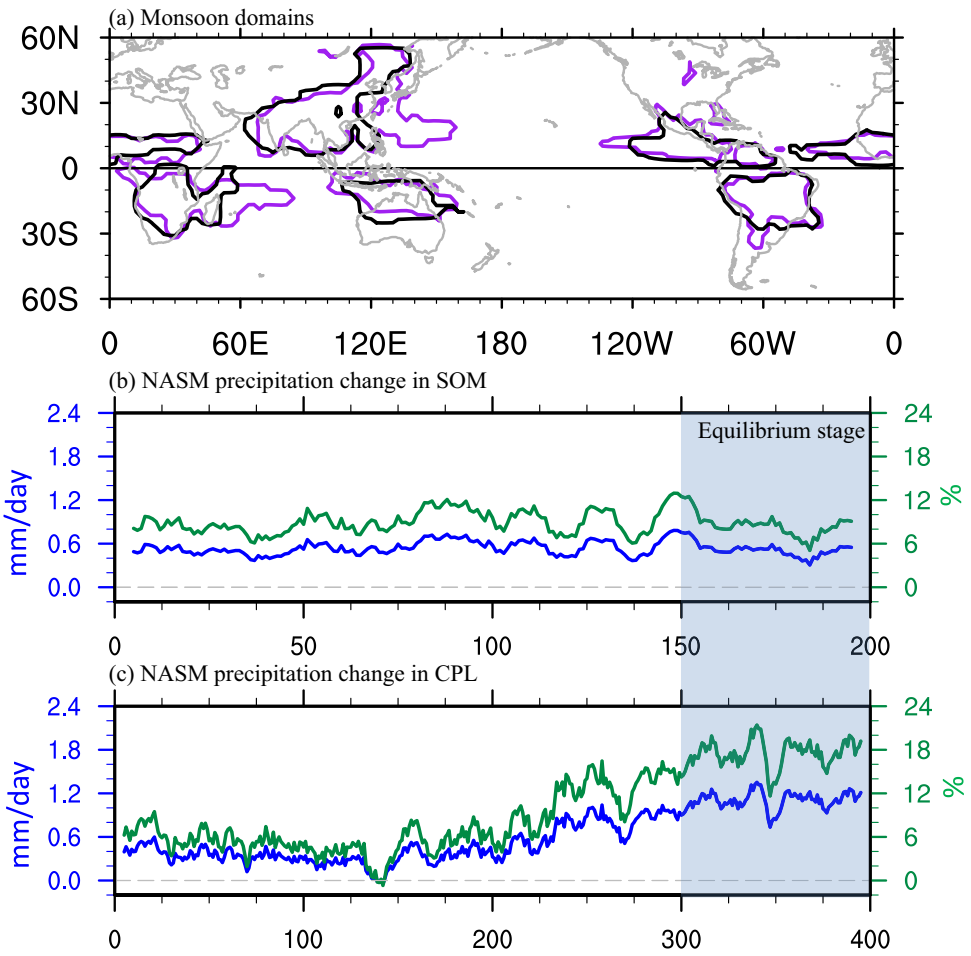

Fig. 2 **a** Monsoon domains in GPCP data (purple contours) and in CTRL simulation (black contours). According to Wang and Ding (2008), the monsoon domains are defined as the region where the local summer precipitation minus local winter precipitation exceeding 2 mm/day and the local summer precipitation exceeds 55% of annual rainfall. **b** Time evolution of changes in North American summer monsoon (NASM) precipitation (mm/day) in SOM runs. Blue curve is for precipitation change while green curve is for its percentage change. **c** Is the same as **b** but for fully coupled (CPL) simulations

2.4 Three-pattern decomposition of global atmospheric circulation

The monsoon circulation is the component of large-scale atmospheric motion. The large-scale atmospheric motion to first order is consist of Rossby wave at mid-high latitudes (Rossby 1939), Hadley and Walker circulation at low latitudes (Trenberth and Solomon 1994; Julian and Chervin 1978). However, these components interact with each other and are hard to be distinguished in the real world. Fortunately, a new method named the three-pattern decomposition of global atmospheric circulation (3P-DGAC) has been introduced by Hu et al. (2017), by which the global atmospheric circulation $\vec{V}$ is decomposed into the horizontal circulation ($\vec{V}'_R$), meridional circulation ($\vec{V}'_H$) and zonal circulation ($\vec{V}'_W$) as follows,

$$\vec{V}' = \vec{V}'_H + \vec{V}'_W + \vec{V}'_R \tag{2}$$

in which,

$$\begin{cases} \vec{V}'_R(\lambda,\theta,\sigma) = u'_R(\lambda,\theta,\sigma)\vec{i} + v'_R(\lambda,\theta,\sigma)\vec{j} \\ \vec{V}'_H(\lambda,\theta,\sigma) = v'_H(\lambda,\theta,\sigma)\vec{j} + \dot{\sigma}_H(\lambda,\theta,\sigma)\vec{k} \\ \vec{V}'_w(\lambda,\theta,\sigma) = u'_W(\lambda,\theta,\sigma)\vec{i} + \dot{\sigma}_W(\lambda,\theta,\sigma)\vec{k} \end{cases} \tag{3}$$

$$\begin{aligned} u'_R &= -\frac{\partial R}{\partial \theta}, \quad & v'_R &= \frac{1}{sin\theta}\frac{\partial R}{\partial \lambda} \\ v'_H &= -\frac{\partial H}{\partial \sigma}, \quad & \dot{\sigma}_H &= \frac{1}{sin\theta}\frac{\partial (sin\theta H)}{\partial \theta} \\ u'_W &= \frac{\partial W}{\partial \sigma}, \quad & \dot{\sigma}_W &= -\frac{1}{sin\theta}\frac{\partial W}{\partial \lambda} \end{aligned} \tag{4}$$

where (λ,θ,σ) is the spherical σ-coordinate system, (u'_R, v'_R), $(v'_H, \dot{\sigma}_H)$ and $(u'_W, \dot{\sigma}_W)$ are the wind vector components of horizonal circulation, meridional circulation, and zonal circulation, respectively. R, H, and W are the stream functions which can be obtained from following equation:

$$\Delta_3 R = \zeta \tag{5}$$

$$\frac{\partial H}{\partial \sigma} = \frac{1}{sin\theta}\frac{\partial R}{\partial \lambda} - v' \tag{6}$$

$$\frac{\partial W}{\partial \sigma} = \frac{\partial R}{\partial \theta} + u' \tag{7}$$

where $\Delta_3 = \frac{1}{sin^2\theta}\frac{\partial^2}{\partial \lambda^2} + \frac{1}{sin\theta}\frac{\partial}{\partial \theta}\left(sin\theta\frac{\partial}{\partial \theta}\right) + \frac{\partial^2}{\partial \sigma^2}$ is the three-dimensional Laplacian in the spherical σ-coordinates and $\zeta = \frac{1}{sin\theta}\frac{\partial v'}{\partial \lambda} - \frac{1}{sin\theta}\frac{\partial (u' sin\theta)}{\partial \theta}$ is the vertical vorticity of the entire atmospheric layer. $(u', v', \dot{\sigma})$ represent the three velocity components in the spherical σ-coordinate system.

3 Changes in NASM precipitation

The time evolution of changes in NASM precipitation under the TP uplift are first shown in Fig. 2b, c. The TP uplift immediately triggers NASM precipitation increase by 0.5 mm/day (6%). This can be seen from the SOM runs (Fig. 2b), in which the precipitation change occurs rapidly right after the TP uplift and remains stable during the following integrations. The fast response of NASM precipitation to the TP uplift can be also seen from CPL runs during the first several decades when the oceanic dynamical process is not fully responded (Fig. 2c). The oceanic dynamical feedbacks further double the NASM precipitation change and lead to precipitation increase to 0.9 mm/day (12%) during the equilibrium stage (Fig. 2c). The spatial distributions of monsoon precipitation change in SOM runs and CPL runs are shown in Fig. 3a, b. The NAM region is characterized by a large extent of significant summer precipitation increase via atmospheric processes (Fig. 3a) and is further amplified by oceanic dynamical feedbacks (Fig. 3b). It is interesting to note that the precipitation is consistently increased over the NAM region by atmospheric processes (Fig. 3a) while the precipitation change induced by oceanic dynamical processes exhibits an out-of-phase pattern with large precipitation increase occurred over central to north NAM region and decrease over south NAM region (Fig. 3b). The changes in surface humidity are also checked here (Fig. 3c, d). The surface air humidity is slightly increased over NAM region in SOM runs (Fig. 3c) while that shows an increase over central to north NAM region and decrease over south NAM region in CPL runs (Fig. 3d). Our finds indicate that the TP

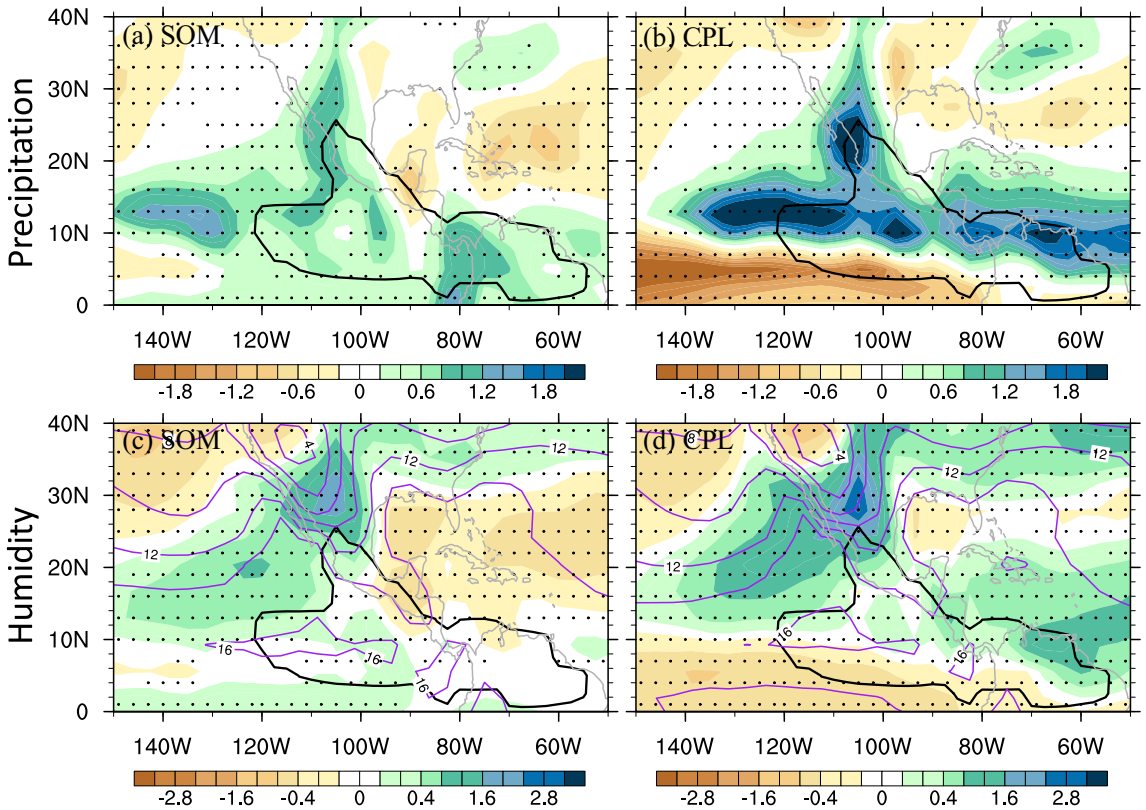

Fig. 3 Equilibrium changes in precipitation and humidity due to the TP uplift: **a** precipitation for SOM runs and **b** precipitation for CPL runs. Units: mm/day. **c** Humidity (shading) for SOM runs and **(d)** humidity (shading) for CPL runs. In **c** and **d**, the purple contours denote the climatological humidity from CTRL_SOM and CTRL, respectively. Units: g/kg. All these values are extracted from boreal summer. The stippling areas indicate the difference exceeding 95% confidence level, determined by a two-tailed Student's t test. The black contours denote the North American monsoon (NAM) region

uplift can increase the NASM precipitation and moisten the most NAM regions.

4 Mechanisms for NASM precipitation change

4.1 Changes in mean climate

To better understand the response of NASM precipitation to the TP uplift, the mean climate changes are also examined here. The TP uplift immediately induces anticyclonic geopotential height anomaly to the north of the TP area and extending from the tropical-subtropical North Atlantic to NAM region, and cyclonic to the south of the TP area, extending to subpolar Pacific and subpolar Atlantic (Fig. 4b). The atmospheric circulation changes are roughly barotropic since the wave pattern at 500 hPa shows resemblance to that at 850 hPa (Yang and Wen 2020). The adjustment of planetary wave pattern is very fast and is also confirmed by our CAM5 model simulation (Figure not shown). More importantly, the atmospheric responses do not change much from SOM runs to CPL runs (Fig. 4b vs d), indicating that the oceanic dynamical processes in the hundreds of years later do not have considerable feedback to the atmospheric circulation. Detailed atmospheric circulation changes are also discussed in Yang et al. (2020), which states that the teleconnection patterns in Fig. 4b, d agree well with those in previous studies (Zhao et al. 2007, 2012) and can be well understood by the classic planetary wave theory in a linear quasigeostrophic system (Hoskins and Karoly 1981).

The high pressure anomaly extending from the tropical-subtropical North Atlantic to NAM region enhances the easterlies over the central American continent, which promotes the evaporation and thus the surface latent heat loss from ocean to atmosphere (Figure not shown), resulting in slightly colder surface air temperature (SAT) around the NAM region in SOM runs (Fig. 4c). In CPL runs, the strengthened trade winds over the eastern Pacific cause poleward Ekman transport and

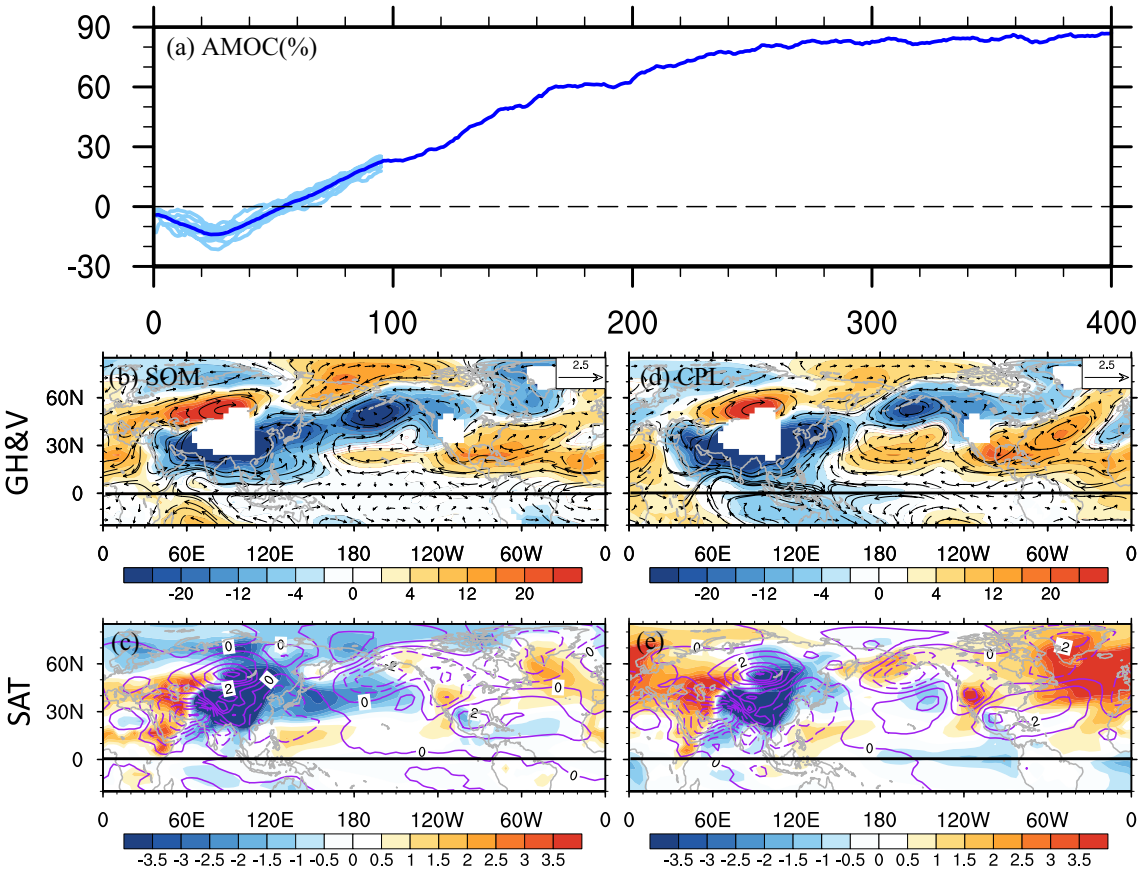

Fig. 4 **a** Time evolution of percentage changes in Atlantic meridional overturning circulation (AMOC) with light blue curves representing results from 10 ensemble CPL runs. The AMOC index is defined as the maximum streamfunction in the range of 0°–10 °C over 20°–70°N in the Atlantic. **b** Equilibrium changes in geopotential height (shading; m) and wind (vector; m/s) at 850 hPa during boreal summer in SOM runs. **c** Equilibrium changes in surface air temperature (SAT; shading; °C) and eddy sea level pressure (contours; hPa) during boreal summer in SOM runs. **(d)** and **(e)** are the same as **(b)** and **(c)**, but for CPL runs

lead to surface current divergence (Figure not shown). The subsurface cold water then upwells to compensate the surface water loss, which results in eastern Pacific (180°W–80°W, 10°S–10°N) cooling (Fig. 4e). In addition, the uplift of the TP can also lead to the establishment of the AMOC (Fig. 4a) by inducing more water vapor transport from the North Atlantic to Pacific Ocean (Yang and Wen 2020). The establishment of the AMOC warms the North Atlantic, western Eurasian continent, as well as the North American continent by generating pronounced heat transport from Southern Hemisphere (SH) to Northern Hemisphere (NH) (Fig. 4e).

4.2 Moisture budget

To understand the processes that drive the NASM precipitation change, the projected changes in precipitation and the first five terms on the right-hand side of Eq. (1) are shown in Figs. 5 and 6 for the SOM and CPL runs, respectively. Note that since we use 50 years of data in SOM runs and 100 years of data in CPL runs, all variables with color shadings are exceeding 95% confidence level determined by a two-tailed Student's t test. For simplifying the figure, we do not add stippling. It is obvious that the dynamic change of vertical moisture advection is the largest contributor to the increased NASM precipitation both in SOM runs and CPL runs, with the magnitude in CPL runs much bigger than that in SOM runs (Figs. 5d, 6d). The enhanced vertical moisture

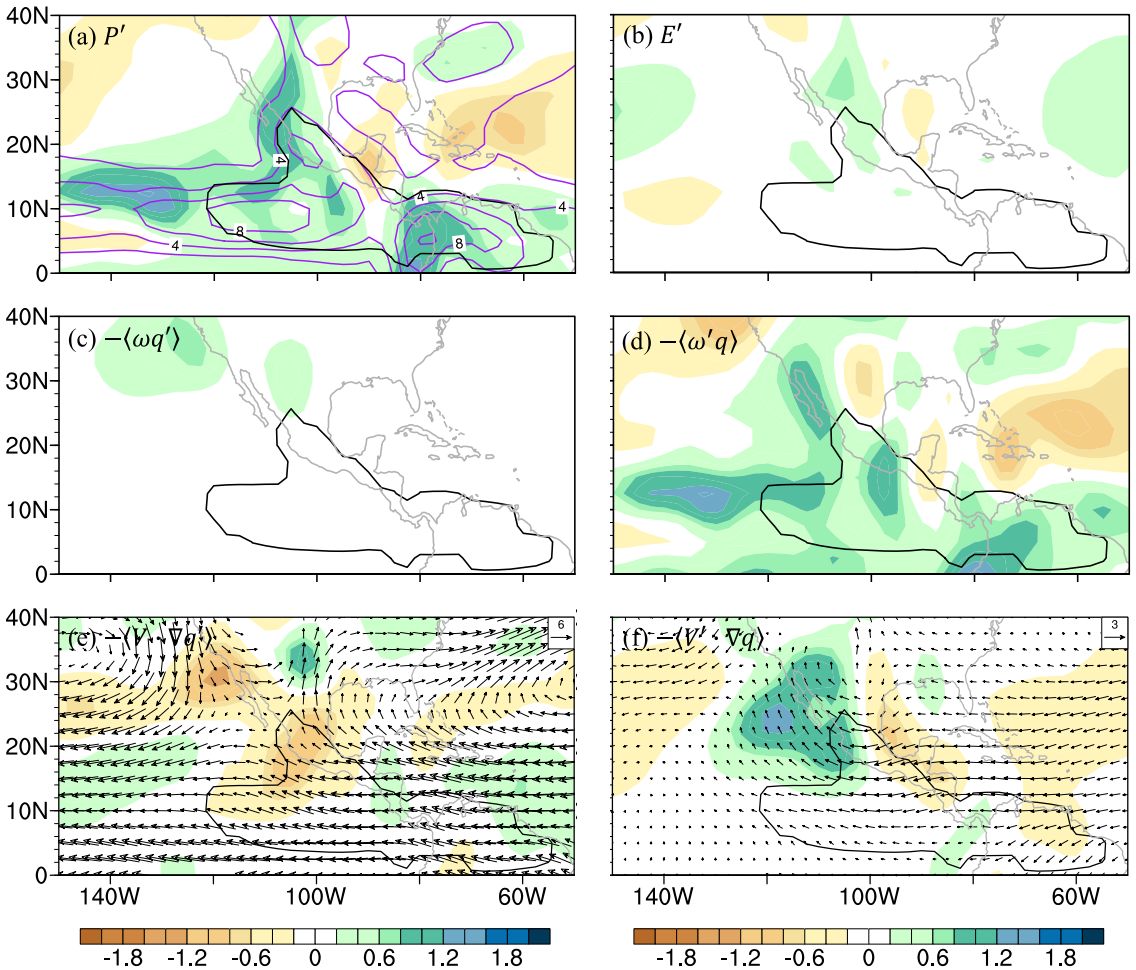

Fig. 5 Equilibrium changes in precipitation and its contributors: **a** precipitation (P', shading), **b** evaporation (E'), **c** thermodynamic component of vertical moisture advection ($-\langle \omega q' \rangle$), **d** dynamic component of vertical moisture advection ($-\langle \omega' q \rangle$), **e** thermodynamic component of horizontal moisture advection ($-\langle V \cdot \nabla q' \rangle$, shading), and **f** dynamic component of horizontal moisture advection ($-\langle V' \cdot \nabla q \rangle$, shading) in SOM runs during boreal summer. Units: mm/day. The black contours denote the NAM region. In **(a)**, the purple contours denote the climatological precipitation in CTRL_SOM simulation. In **(e)**, the vectors (units: m/s) denote the climatological winds at 850 hPa in CTRL_SOM simulation. In **(f)**, the vectors (units: m/s) denote the wind difference between CTRL_SOM and NoTP_SOM

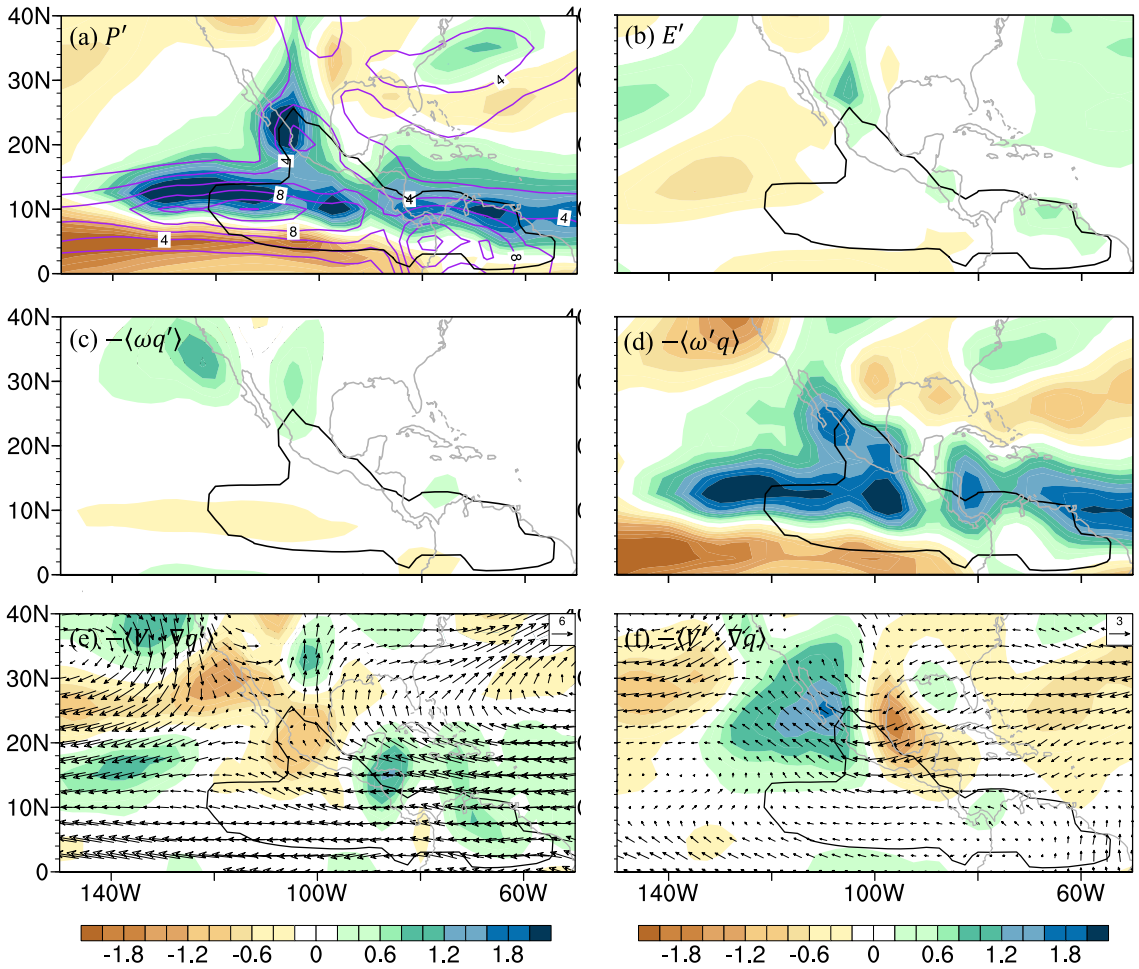

Fig. 6 Same as Fig. 5 but for CPL runs

advection is due to the increased upward motion, a point to be returned later. The evaporation term is hardly changed because the TP-uplift induced surface temperature change over this region is small (Fig. 4c, e). The weak temperature change also contributes to the hardly changed thermodynamic component of vertical moisture advection (Figs. 5c, 6c). The thermodynamic and dynamic changes in horizontal moisture advection are both uncertain and small over the NAM region (Figs. 5e, f, 6e, f), consistent with previous studies that the horizontal moisture advection is usually less important than vertical moisture advection to precipitation (Chou et al. 2009; Zhang et al. 2017). The contribution of these terms to NASM precipitation change are summarized in Fig. 7a. The dynamic change of vertical moisture advection term nearly contributes 100% precipitation increase in SOM runs and CPL runs, respectively, which is undoubtedly the dominant term for NASM precipitation change. Based on Eqs. (2)–(7), the dynamic change of vertical moisture advection term can be further broken into vertical moisture advection due to meridional circulation and zonal circulation change (Fig. 7b). The increased dynamic change of vertical moisture advection term ($-\langle\omega' q\rangle$) largely comes from meridional circulation change ($-\langle\omega_H{}' q\rangle$). The zonal circulation change appears to suppress the NASM precipitation increase ($-\langle\omega_W{}' q\rangle$).

4.3 Mean vertical velocity and 3P-DGAC

To understand the atmospheric circulation change, the mean atmospheric vertical velocity and precipitation during boreal summer are first shown in Fig. 8. In the annual mean state of observations, the large-scale upward motion is expected in the tropics, with centers near equatorial Africa, the Indian Ocean, the western Pacific, the eastern Pacific, the South America, and the Atlantic Ocean (Fig. 8a) (Chen et al. 2014; Cheng et al. 2020). During boreal summer, the upward motion gets stronger in the NH and weaker in the SH (shading in Fig. 8b compared with that in Fig. 8a), indicating the large-scale northward shift of Intertropical Convergence Zone (ITCZ) (contours in Fig. 8b compared with that in

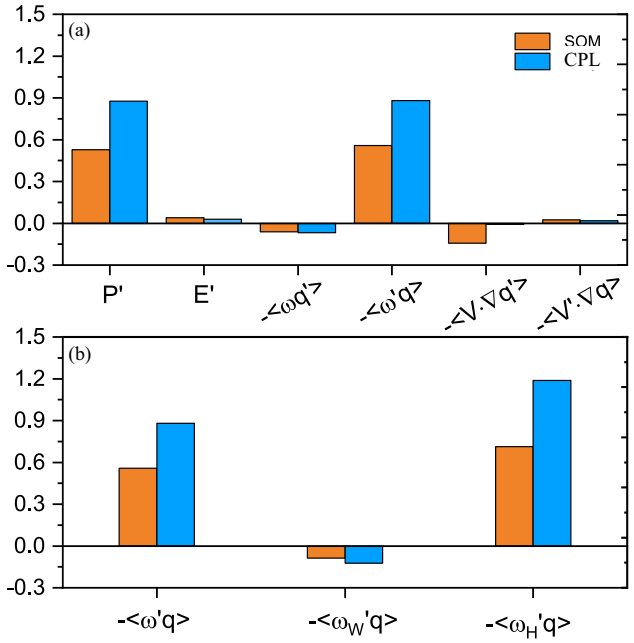

Fig. 7 Bar char for the mean changes in **a** precipitation and its contributors and **b** dynamic component of vertical moisture advection and its contributors. Orange bar is for SOM runs and blue bar is for CPL runs. In **a**, The meaning of labels at x-axis is the same as that in Fig. 4. In **b**, $-<\omega_W^{'}q>$ denotes the dynamic term due to zonal circulation change and $-<\omega_H^{'}q>$ denotes the dynamic term due to meridional circulation change. Units: mm/day. All values are from boreal summer

Fig. 8a). These features are also captured in our CTRL and CTRL_SOM simulation (Fig. 8c, d). Strong upward motion in the tropics is associated with deep convection and corresponds to above-normal precipitation in these regions while strong descending motion in the subtropics suppresses the convection and corresponds to the aridity (contours in Fig. 8a–d) (Chen et al. 2014). Comparing CTRL_SOM and NoTP_SOM, the upward motion is strengthened over the NAM region (shading in Fig. 8h), resulting in more precipitation over there (contours in Fig. 8h). Comparing CTRL and NoTP, the TP uplift leads to a northward shift of the maximum upward motion over the NAM region, results in enhanced upward motion and thus the increased precipitation in the northern area of NAM region, and weakened upward motion and thus the decreased precipitation in the southern area of NAM region (shading and contours in Fig. 8g).

Previous works suggest that the tropical overturning circulation consists of a couple of orthogonal overturning circulation, that is, meridional and zonal circulations (Hu et al. 2018). Based on 3P-DGAC method, the vertical wind can be decomposed into two parts, the vertical winds related to meridional circulation and zonal circulation. i.e., $\omega = \omega_H + \omega_W$, where ω, ω_H and ω_W represent the total vertical wind, the vertical wind of meridional circulation and that of zonal circulation, respectively (Hu et al. 2018). The vertical velocity and its meridional and zonal components are shown in Fig. 9. In the real world, the maximum upward motion of meridional circulation are located over equatorial Africa, the Indian Ocean, the western Pacific, the eastern Pacific, and the tropical North Atlantic Ocean, indicating the ascending branch of regional Hadley circulations (Fig. 9b, f). All these regional Hadley circulations are characterized by two circulations with rising branch in the tropical regions and sinking branch in the subtropics of both hemispheres (Fig. 9b, f) (Cheng et al. 2020). For zonal circulation, there are three main centers over the Indian Ocean, the western Pacific Ocean and the western Atlantic Ocean, representing the three rising branches of Walker circulation (Fig. 9c, g). The sinking branches of Walker circulation are located in the western Indian Ocean, the eastern Pacific Ocean and the eastern Atlantic Ocean. The residual term is very small and can be negligible in latter discussion (Fig. 9d, h). The decomposition results of vertical velocity are similar to previous works (Hu et al. 2017; Cheng et al. 2020). The traditional method to define the Hadley circulation is based on the zonal average, so the contribution of the zonal component vanishes [$\omega_W = 0$] and [ω] contains only [ω_H]. Thus, it is appropriate to use zonal averaged total vertical velocity to represent the Hadley circulation in the previous studies (Wen et al. 2018). However, it is incorrect to use regional total vertical velocity, i.e., the vertical wind between 80° W and 10° W to represent the regional Hadley circulation since the ω_W is not zero (Fig. 9c, g). In addition, the traditional definition of the Walker circulation is restricted to the tropical region and $\langle\omega\rangle_{5^\circ S}^{5^\circ N}$ is often used to calculate the Walker circulation. In this case, the $\langle\omega_H\rangle_{5^\circ S}^{5^\circ N} \neq 0$ (Fig. 7b, f), which means that the contribution of the meridional circulation is included in the vertical velocity of the Walker circulation. So, when analyzing the meridional circulation (zonal circulation), the vertical wind of meridional component (zonal component) should be used. By using this method, we can analyze the regional meridional circulation and zonal circulation.

4.4 Mechanisms for NASM precipitation change

The changes in vertical velocity and its meridional component and zonal component during boreal summer are shown in Fig. 10 to illustrate the mechanisms that govern the NASM precipitation response. As discussed in Sect. 4.3, the NAM region is characterized by an enhanced ascending motion (shading in Fig. 8g, h), which is dominated by the meridional circulation change both in SOM runs and CPL runs (Fig. 10b, e). However, the mechanisms may be different. In SOM runs, the TP uplift generates enhanced upward motion of meridional component over the NAM region and its surrounding regions, which dominates the total vertical

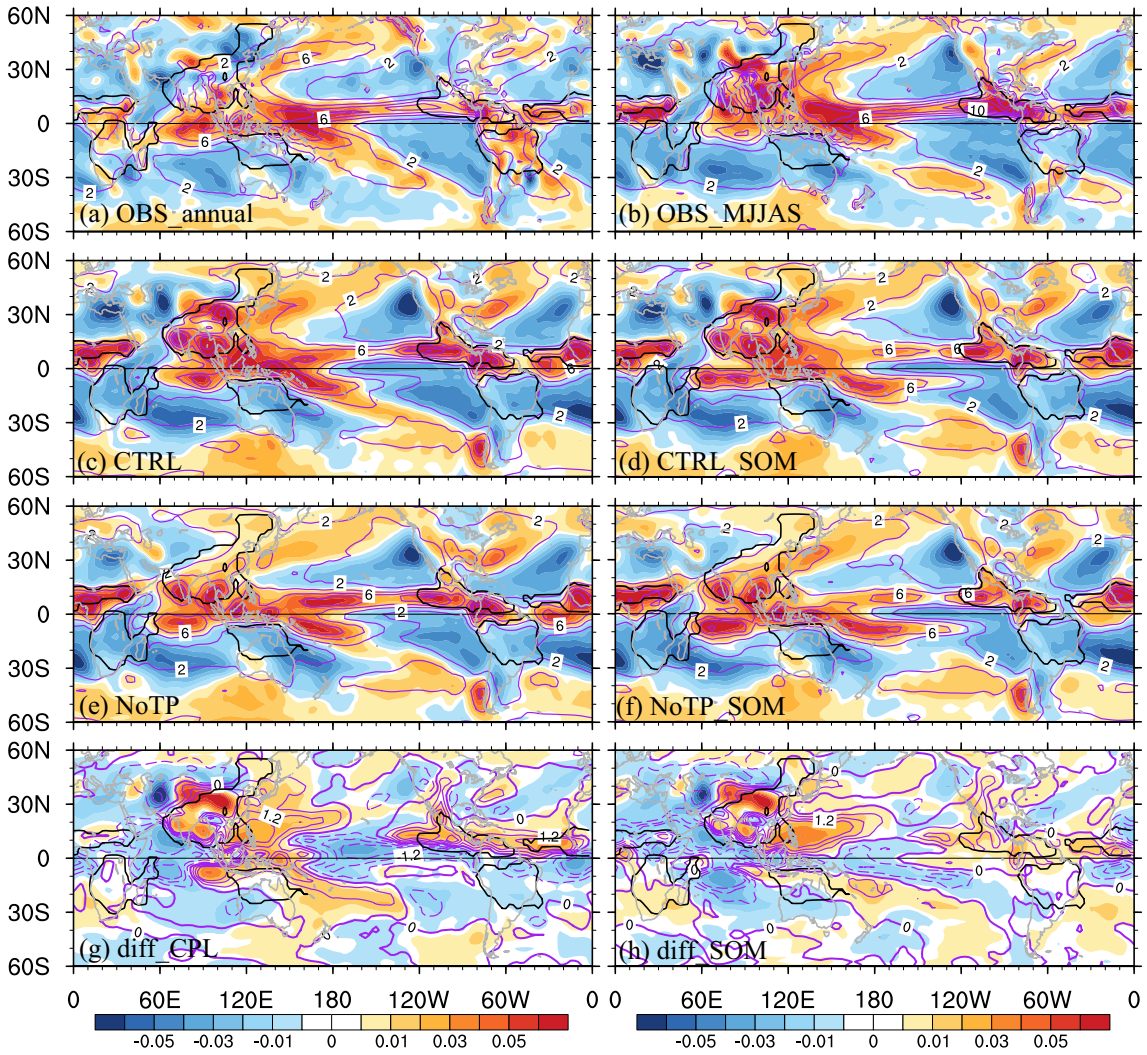

Fig. 8 Vertical velocity (Pa/s; shading) and precipitation (mm/day; contours). **a** and **b** Are for the observation data during annual mean and boreal summer, respectively. The vertical velocity is from NCEP-2 while the precipitation is from GPCP during 1979–2018. **c–f** Are for CTRL, CTRL_SOM, NoTP and NoTP_SOM respectively. **g** Is the difference between **(c)** and **(e)** while **(h)** is the difference between **(d)** and **(f)**. In **(c–h)**, all these values are extracted from boreal summer

wind change (Fig. 10b) and results in increased NASM precipitation (Fig. 7b). Compared to SOM runs, the enhanced upward motion in CPL runs is located further north with abnormal descending motion at the south tip of it, indicating that the meridional circulation shifts northward (Fig. 10e). The changes in upward motion of zonal component over the NAM region is very small and uncertain compared with that of meridional component.

4.4.1 Mechanisms in SOM runs: the atmospheric teleconnection response

The change in meridional component of vertical velocity over the NAM region refers to the regional Hadley circulation (HC) response. Here, we define the regional HC over eastern Pacific-Atlantic sector as spanning 120°W-40°W (red box in Fig. 10b, e) and plot it in Fig. 11. In SOM runs, the summer HC gets strengthened in both hemispheres under the TP uplift with the magnitude in NH much stronger than that in SH (Fig. 11a). The strengthened HC in NH results in enhanced convection over the NAM region and thus the increased summer precipitation (Fig. 7b). The strengthened regional HC in SOM runs is related to the adjustment of planetary waves (Fig. 4b). The abnormal positive geopotential height extending from the tropical-subtropical North Atlantic to the NAM region is accompanied by the northeasterly wind at the south tip of it, which results in stronger regional HC over NAM region by enhancing the horizontal momentum flux from the surface into the atmosphere (Cook et al. 2003). Actually, the negative–positive geopotential

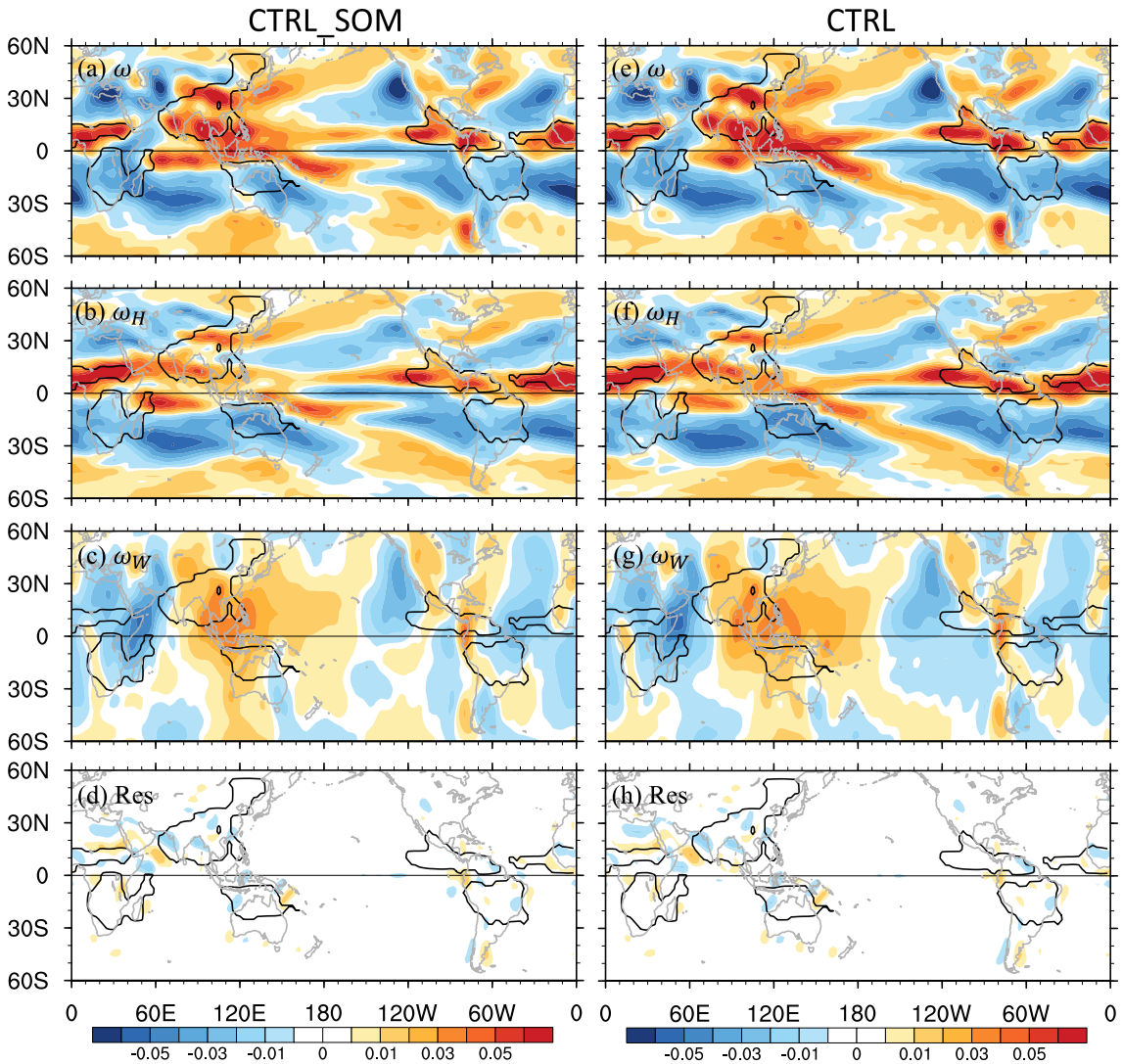

Fig. 9 **a** Total vertical velocity and its **b** meridional component, **c** zonal component and **d** residual in CTRL_SOM at 500 hPa during boreal summer. **(e)–(h)** Are the same as **(a)–(d)** but for CTRL. The decomposition are based on 3P-DGAC method. Units: Pa/s. The value of vertical velocity have been multiplied by – 1 from its original value, so the positive value is for upward motion

anomaly over the North Atlantic is not unlike the positive phase of the North Atlantic oscillation, which is always associated with the enhanced HC (Cook et al. 2003; Iqbal et al. 2019; Qiao et al. 2020).

4.4.2 Mechanisms in fully coupled runs: the indirect impact from the altered AMOC

In CPL runs, the TP uplift induces a northward shift of HC in NH, resulting in increased upward motion over the NAM region (Fig. 11c, d). The northward shift of HC in CPL runs can be understood by the meridional temperature gradient change. The uplift of the TP induces the establishment of AMOC (Fig. 4a), which brings substantial heat northward to warm the NH, especially over the North Atlantic and North American continent. The profound warming over mid-high latitudes reduces the meridional temperature gradient, which leads to a northward shift of HC (Bush and Philander, 1999; Yang et al. 2017; D'Agostino et al. 2017; Liu and Zhou, 2017). Actually, there is close coupling between sea surface temperature and precipitation in the tropics (Xie et al. 2010). Over the eastern Pacific-Atlantic section in CPL runs, the SST warming occurs north of 10°N while cooling occurs south of 10°N (Fig. 12c). The asymmetric SST change and thus the weakened meridional temperature gradient lead to a profound upward motion around 10°N in the real world (Fig. 8c), otherwise the upward motion is located further south (Fig. 8e). This is consistent with the northward shift of precipitation (Fig. 12c). However, in SOM runs, the

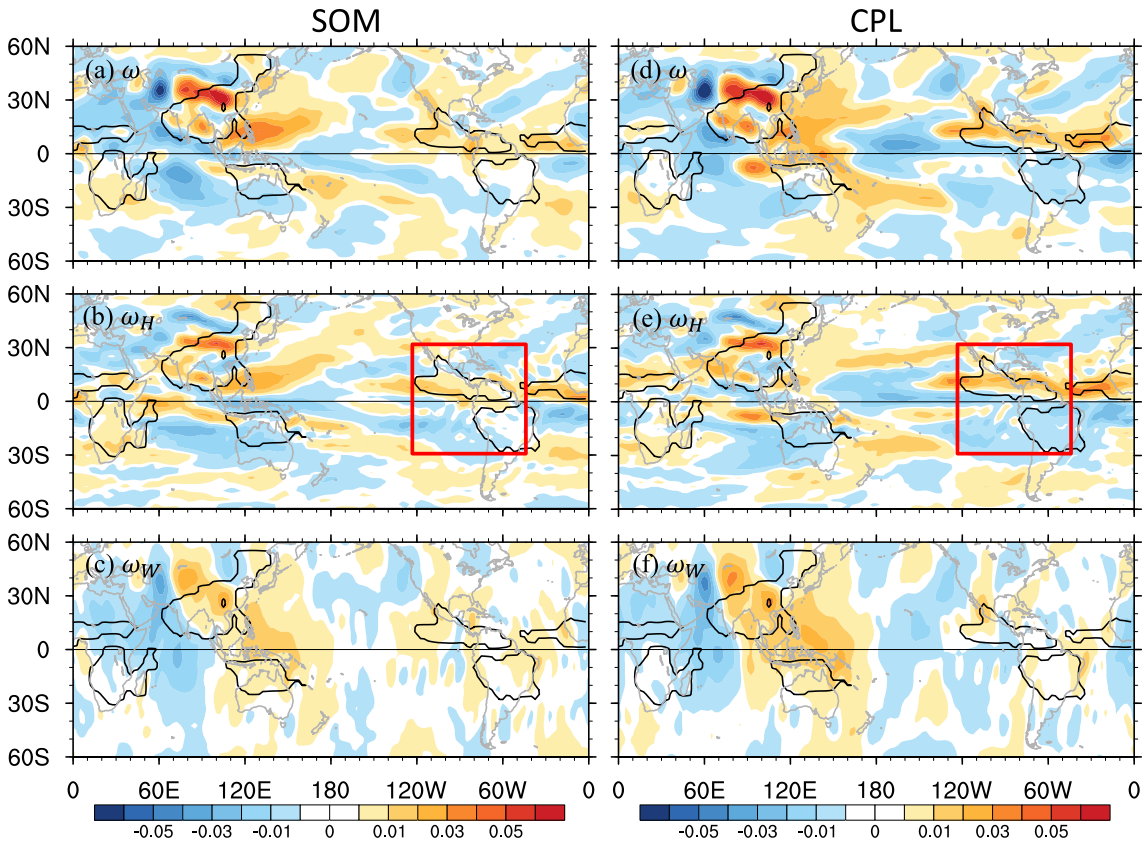

Fig. 10 Equilibrium changes in **a** total vertical velocity (units: Pa/s) and its **b** meridional component and **c** zonal component at 500 hPa during boreal summer in SOM runs, respectively. **d–f** Are the same as **(a)-(c)** but for CPL runs. The red rectangle outlines the eastern Pacific-Atlantic section (120°W–40°W). The value of vertical velocity has been multiplied by – 1 from its original value, so the positive value is for upward motion

meridional temperature change is relatively small, so the HC hardly shifts.

The northward shift of precipitation in CPL runs can also be understood by regional ITCZ shift. The ITCZ positions are shown in Fig. 12. The ITCZ over the eastern Pacific-Atlantic Sect. (120°W-40°W) is related to the NASM precipitation. In this section, the mean position of ITCZ in CTRL_SOM is at 6.7°N, with no shift in NoTibet_SOM (Table 1 or red and orange dots in Fig. 12b). We further split the eastern Pacific-Atlantic section into eastern Pacific (120°W–80°W) and Atlantic Sect. (80°W–40°W) and find that the ITCZ is no shift in these two regions in SOM runs under the TP uplift (Table 1). However, in CPL runs, the ITCZ shifts northward by 2.2°N over the eastern Pacific-Atlantic section, with 1.3°N northward shift over the eastern Pacific and 2.7°N northward shift over the western Atlantic. The northward shift of ITCZ in CPL runs results in substantial precipitation increase over the central to north NAM region and decrease over the southern tip of the NAM region (Fig. 12d).

The northward shift of ITCZ over the eastern Pacific-Atlantic section can be explained by regional atmospheric energy budget (Boos and Korty 2016; Lintner and Boos 2019). The energy input into the atmosphere is shown in Figs. 13,14,15. In the TP region, the radiation fluxes at the TOA are remarkable reduced (Fig. 13a). The TP uplift generates anomalous low pressure over the TP region, which promotes the convection and moisture convergence, and thus the clouds formation (Fig. 13e, f). The increased clouds increase the planetary albedo (Fig. 13d), which hinder the incoming solar radiation (SW) and outgoing longwave radiation (LW) (Fig. 13b, c). In contrast to the heat fluxes reduction over the TP, the North Atlantic experiences a heat flux increase, with net incoming SW and outgoing LW all enhanced (Fig. 13a–c). The increased net downward SW is attributed to the low cloud reduction while the increased outgoing LW is due to surface warming instead of high cloud change (Fig. 13f). These processes are detailed described in Yang et al (2020). At the surface, the net heat fluxes into the atmosphere over the TP region are nearly unchanged, with the SW increase perfectly compensating the LW decrease (Fig. 14a–c). The SW increase is due to enhanced surface albedo, which can reflect more SW from surface to the atmosphere. The LW reduction is caused by surface cooling

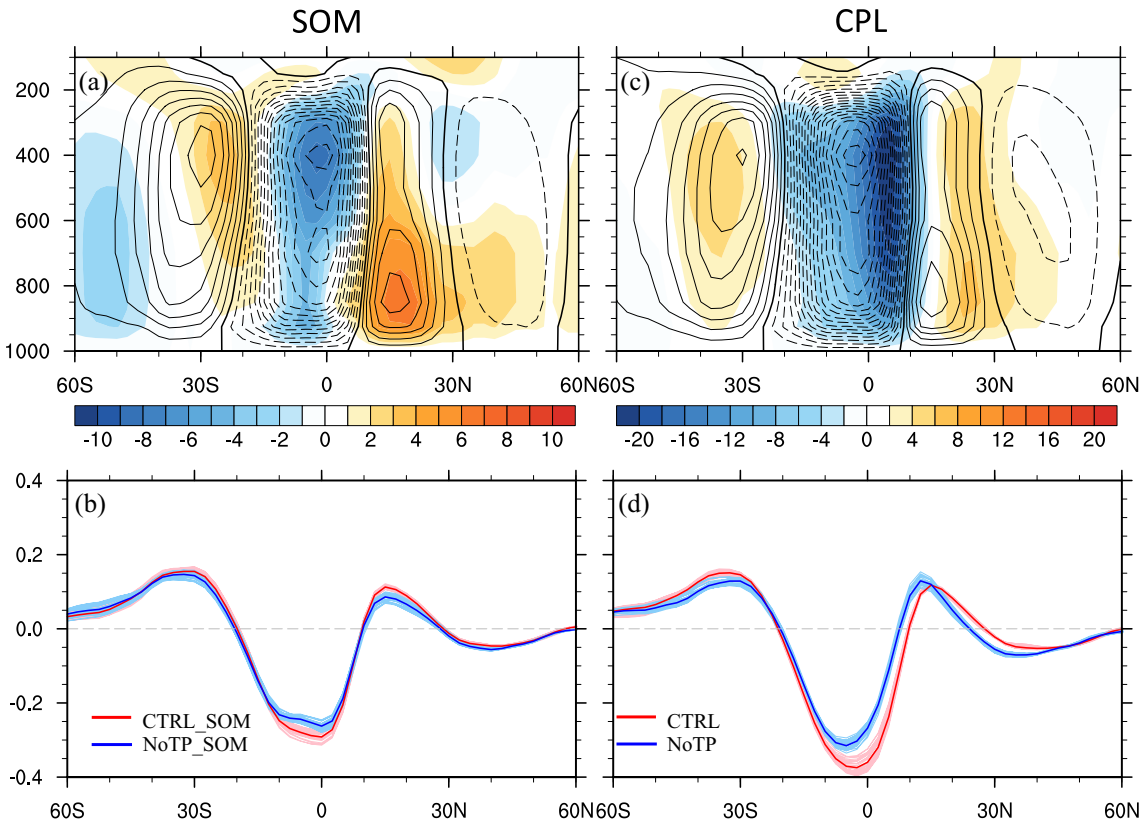

Fig. 11 Mass stream function (10^9 kg/s) averaged between 120°W and 20°W during boreal summer in **(a)** SOM runs and **(c)** fully coupled runs. The black contours denote the mean values in a word with the TP while the shadings denote the difference. **b** and **d** Are the vertical averaged mass stream function in **(a)** and **(c)** correspondingly. In **(b)** and **(d)**, thick curves represent 50-year-mean and 100-yearr-mean values respectively while light color curves are for individual years

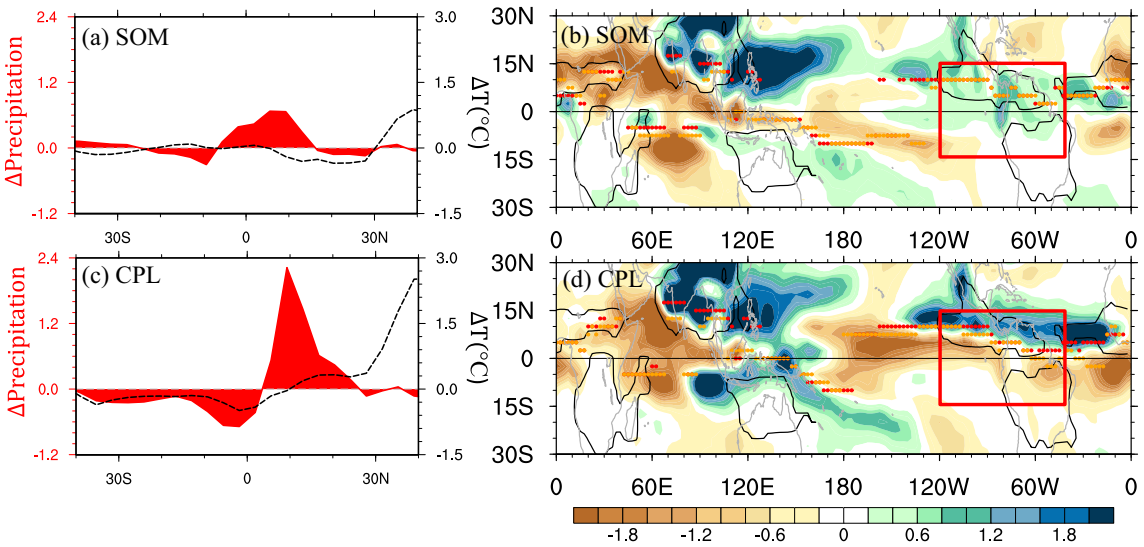

Fig. 12 **a** and **c** are equilibrium changes in zonal mean precipitation (mm/day; red curve) and SAT (°C; dashed black curve) during boreal summer over the eastern Pacific-Atlantic section in SOM and CPL runs, respectively. **b** and **d** Are equilibrium changes in precipitation (mm/day; shading) and the location of Intertropical Convergence Zone (ITCZ) during boreal summer in SOM and CPL runs, respectively. The orange dots are for ITCZ position in a world without the TP while the red dots are for ITCZ position in a world with the TP. The ITCZ position is defined as the location of the maximum precipitation at low latitudes (Mamalakis et al. 2021). The red rectangle outlines the eastern Pacific-Atlantic section

Table 1 The ITCZ position

Experiments	120°W–40°W	120°W–80°W	80°W–40°W
CTRL_SOM	6.7	9.0	4.9
NoTibet_SOM	6.7	9.0	4.9
CTRL	6.0	9.0	3.7
NoTibet	3.8	7.7	1.0

(Fig. 4e). In the North Atlantic, the surface net heat fluxes into the atmosphere are remarkable increased (Fig. 14a), which is predominately caused by increased LW and latent heat flux (Fig. 14c, f). The AMOC establishment generates profound warming over the North Atlantic, which allows more LW loss from ocean to atmosphere (Fig. 14c). The warming can also enhance the ocean surface evaporation and thus the latent heat flux into the atmosphere (Fig. 14f). The energy flux change at the TOA and surface leads to energy loss over the Asian continent and energy gain over the North Atlantic (Fig. 15a) while the energy flux change over the SH is very small (Fig. 15). The inter-hemispheric energy asymmetry over the eastern Pacific-Atlantic section results in an increase of southward atmospheric energy transport at the equator (Fig. 15b), which is consistent with the revealed northward shift of the ITCZ (Fig. 12d). In addition, the atmospheric energy transport over tropics largely depends on the mean circulation change, i.e., the HC. Thus, the abnormal southward energy transport is completed by the northward shift the HC (Fig. 11c, d).

Actually, The eastern Pacific exhibits a significant cooling in our study (Fig. 4e), which may also contribute to the northward shift of eastern Pacific ITCZ. The tropical eastern Pacific cooling is not unlike the La Niña conditions. Previous studies demonstrate that the interannual variations of the ITCZ associated with ENSO are most pronounced over the Pacific (Dai and Wigley 2000; Adams et al. 2016a). These variations are characterized by an equatorward shift of the ITCZ during El Niño episodes and a poleward shift during La Niña episodes (Adams et al. 2016a, b). Our results are quite consistent with these prior works, in which we show that the La Niña-like SST change over tropical Pacific is followed by northward ITCZ shift over the eastern Pacific.

5 Summary and discussion

In this study, the impact of the TP topography on NASM precipitation is investigated in SOM runs and CPL runs. The TP uplift is found to enhance the NASM both directly via the atmospheric teleconnection and indirectly via the impact of the altered AMOC. First, the TP uplift alters the planetary wave patterns and generates an enhanced Atlantic

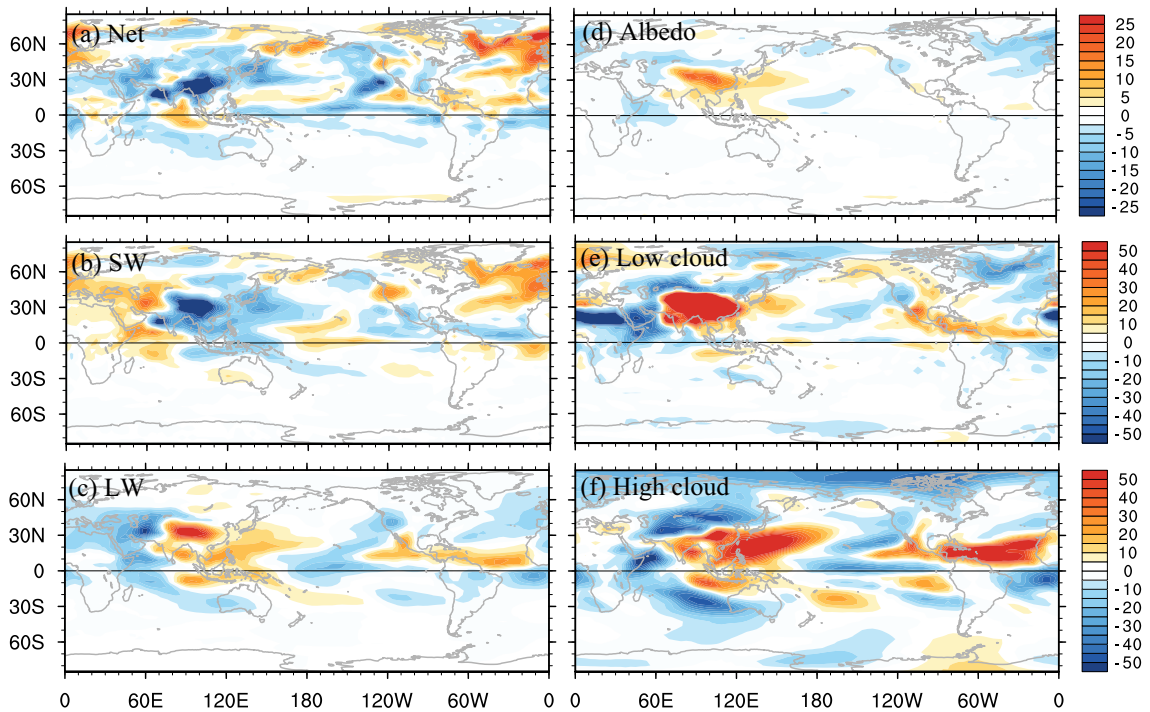

Fig. 13 Equilibrium changes in radiation flux and clouds during boreal summer due to the TP uplift: **a** net radiation flux and **b** shortwave radiation flux (SW) and **c** longwave radiation flux (LW) at the TOA. Units: W/m^2. Positive (negative) value represents downward (upward) flux. **d–f** Are planetary albedo, low cloud, and high cloud, respectively. Units: percentage (%)

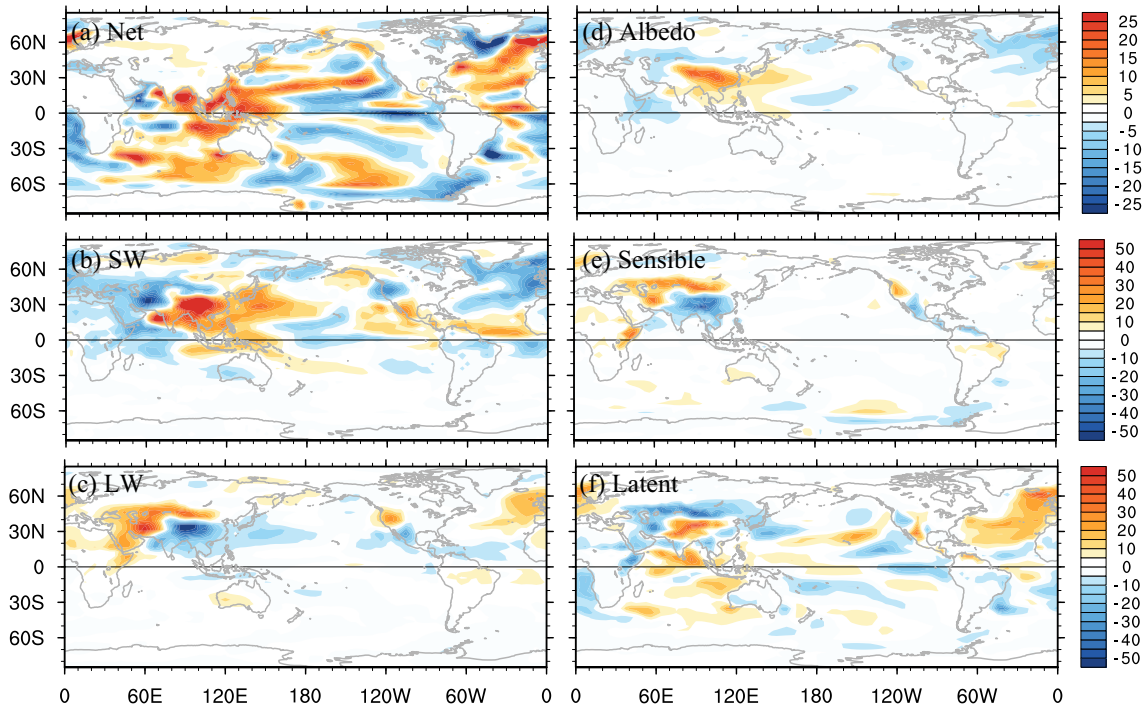

Fig. 14 Equilibrium changes in heat flux during boreal summer due to the TP uplift: **a** net radiation flux and **b** SW, **c** LW, **e** sensible heat flux and **f** latent heat flux at the surface. Units: W/m^2. Positive (negative) value represents upward (downward) flux. **d** Is planetary albedo. Units: percentage (%)

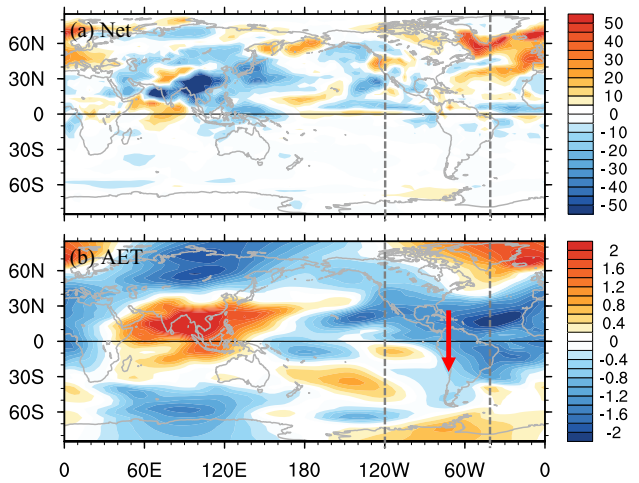

Fig. 15 **a** Equilibrium changes in net energy input into the atmosphere during boreal summer. Units: W/m^2. Positive value represents heat flux incoming into the atmosphere. **b** Changes in the divergent meridional component of the atmospheric energy transport (AET) during boreal summer. Units: 10^7 W/m. The red arrow represents the southward transport of AET. The calculation for AET follows Mamalakis et al. (2021)

subtropical high, which strengthens the northeasterlies over tropical eastern Pacific-Atlantic section and thus the enhanced regional HC there. The strengthened upward motion leads to enhanced convection and thus the increased NASM precipitation. These processes are completed within several decades due to atmospheric adjustment. Second, the TP uplift can also enhance the NASM rainfall indirectly by triggering the AMOC establishment, which reduces the meridional temperature gradient, leading to a northward shift of the HC. The northward shift of the HC shifts the center of the ascending motion northward to 10°N and substantially enhance the convection over the NAM region, and then, the NASM precipitation. Actually, the pattern of SAT response over the tropical Atlantic in CPL runs is not unlike the Atlantic meridional mode, which is characterized by meridional SST gradients over the tropical Atlantic, and is reported to regulate the position of the ITCZ and Hadley circulation (Chang et al. 1997; Chiang et al. 2002; Chiang and Vimont 2004). This study shows a robust relationship between the topography of the TP and NASM precipitation, complimentary to previous perspective that TP uplift can substantially change rainfall over the Asian monsoon region.

The topography of the TP in shaping the NASM precipitation is helpful for our understanding of the TP's role in the global climate system. Previous studies mostly focus on the TP impact on Asian monsoon precipitation, while we highlight the connection between the TP topography and North American monsoon precipitation and show that the existence of the TP leads to more humid NAM climate. The results

obtained in this study may be model dependent. For example, the model resolution is quite low in this study, which cannot well capture the realistic topography, synoptic circulation, and mesoscale circulation that have been reported to be crucial for adequately representing the NAM (Adams et al. 1997; Pascale et al. 2016, 2019; Varuolo-Clarke et al. 2019). The NAM response to external forcings is also sensitive to SST biases (Pascale et al. 2016, 2017). However, the excessive cold tongue is a common feature in general circulation model (Wen et al. 2020), which may alter the response of NASM precipitation to TP uplift. In addition, we only consider the total precipitation change over NAM region in this study. Actually, changes in the timing and seasonal distribution of precipitation may also have significant ecological and societal consequences (Cook et al. 2013), which deserves more investigation in the future. Although this is a highly idealized modeling study with some model limitations, this work helps explain the quantitative role of the TP in the real world. The evolution of tropical American climate during the geological time period is not only related to regional circulation change, but also links to Asian high land regions.

Our modeling results may have applications for paleoclimate studies. For example, previous works use fossil flowers to reconstruct the Miocene climate over south Mexico and show that the environmental conditions of the Chiapas is warmer and drier than in the present (Hernández et al. 2020), which is consistent with our study. Su et al. (2018) use climate models and show that water vapor is divergent over tropical American continent without the TP, indicating that the tropical American continent is much drier in a world without the TP. Huber and Goldner (2012) analyze the Eocene monsoons and show that a high TP can generate precipitation increase over the central American region, consistent with this study. As suggested in previous works, the elevated TP heating can affect the Asian-Pacific Oscillation intensity, with positive tropospheric temperature deviation over the Eurasian continent and negative tropospheric temperature deviation over the central and eastern North Pacific, as well as the Atlantic Ocean (Nan et al. 2009; Duan et al. 2012). The teleconnection pattern is also found in our studies.

This work may also have some implications on modern climate. The TP uplift can induce thermal heating at middle troposphere by lapse rate relationship, which is similar to the rapid warming over the TP in the past decades (Duan and Xiao 2015). There are many studies show that the TP heating could enhance East Asian summer rainfall (Wang et al. 2008), the monsoon rainfall variability in Pakistan (Wang et al. 2019). In addition to the climate change over the Asian continent, the TP heating may also trigger the warming and high-pressure anomaly over the North Atlantic (Zhao et al. 2012; Lu et al. 2018). The high pressure anomaly over the North Atlantic may enhance the upward motion over the NAM region and result in enhanced NAM precipitation. However, The role of TP heating on NAM climate lacks direct investigation, more model studies and observations should be considered to unravel the role of TP in shaping the NAM climate.

Acknowledgements This work is supported by the NSF of China (Nos. 91737204, 41725021, 41376007, 41630527, 4201101394, 42005012, 41971108, and 91437218), the Fundamental Research Funds for the Central Universities (Nos. B210201009), and the Natural Science Foundation of Jiangsu Province (Nos. BK20201058). The experiments were performed on the supercomputers at the Chinese National Supercomputer Centre in Tianjin (Tian-He No. 1). We thank three anonymous reviewers for their efforts to substantially improve this article.

References

Adam O, Bischoff T, Schneider T (2016a) Seasonal and interannual variations of the energy flux equator and ITCZ Part I: Zonally averaged ITCZ position. J Clim 29(9):3219–3230

Adam O, Bischoff T, Schneider T (2016b) Seasonal and interannual variations of the energy flux equator and ITCZ. Part II: Zonally varying shifts of the ITCZ. J Clim 29(20):7281–7293

Adams D, Comrie A (1997) The north American monsoon. Bull Am Meteor Soc 78(10):2197–2214

An Z, Kutzbach J, Prell W et al (2001) Evolution of Asian monsoons and phased uplift of the Himalaya-Tibetan plateau since Late Miocene times. Nature 411(6833):62–66

Boos WR, Korty RL (2016) Regional energy budget control of the intertropical convergence zone and application to mid-Holocene rainfall. Nat Geosci 9(12):892–897

Boos WR, Kuang Z (2010) Dominant control of the South Asian monsoon by orographic insulation versus plateau heating. Nature 463(7278):218–222

Bush ABG, Philander SGH (1999) The climate of the Last Glacial maximum: results from a coupled atmosphere-ocean general circulation model. J Geophys Res Atmos 104(D20):24509–24525

Castro CL, McKee TB Sr, Pielke RA (2001) The relationship of the North American monsoon to tropical and North Pacific sea surface temperatures as revealed by observational analyses. J Clim 14(24):4449–4473

Cerling TE, Harris JM, Ambrose SH et al (1997) Dietary and environmental reconstruction with stable isotope analyses of herbivore tooth enamel from the Miocene locality of Fort Ternan, Kenya. J Hum Evolut 33(6):635–650

Chang P, Ji L, Li H (1997) A decadal climate variation in the tropical Atlantic Ocean from thermodynamic air-sea interactions. Nature 1385(6616):516–518

Chen J, Bordoni S (2014) Orographic effects of the Tibetan Plateau on the East Asian summer monsoon: an energetic perspective. J Clim 27(8):3052–3072

Chen S, Wei K, Chen W et al (2014) Regional changes in the annual mean Hadley circulation in recent decades. J Geophys Res: Atmos 119(13):7815–7832

Cheng J, Hu S, Gao C et al (2020) On the discrepancies in the changes in the annual mean Hadley circulation among different regions and between CMIP5 models and reanalyses. Theoret Appl Climatol 141(3):1475–1491

Chiang J, Vimont D (2004) Analogous Pacific and Atlantic meridional modes of tropical atmosphere–ocean variability. J Clim 17(21):4143–4158

Chiang J, Kushnir Y, Giannini A (2002) Deconstructing Atlantic Intertropical Convergence Zone variability: Influence of the local cross-equatorial sea surface temperature gradient and remote forcing from the eastern equatorial Pacific. *Journal of Geophysical Research: Atmospheres*, 107(D1): ACL 3–1-ACL 3–19.

Chou C, Neelin JD, Chen CA, Tu JY (2009) Evaluating the "'rich-get-richer"' mechanism in tropical precipitation change under global warming. J Clim 22:1982–2005

Cook KH (2003) Role of continents in driving the Hadley cells. J Atmos Sci 60(7):957–976

Cook BI, Seager R (2013) The response of the North American Monsoon to increased greenhouse gas forcing. Journal of Geophysical Research: Atmospheres 118(4):1690–1699

D'Agostino R, Lionello P, Adam O et al (2017) Factors controlling Hadley circulation changes from the Last Glacial Maximum to the end of the 21st century. Geophys Res Lett 44(16):8585–8591

Dai A, Wigley T (2000) Global patterns of ENSO-induced precipitation. Geophys Res Lett 27(9):1283–1286

de Jesús Hernández-Hernández M, Cruz JA, Castañeda-Posadas C (2020) Paleoclimatic and Vegetation Reconstruction of the Miocene Southern Mexico using Fossil Flowers. J S Am Earth Sci 104:102827

Duan A, Wu G (2006) Change of cloud amount and the climate warming on the Tibetan Plateau. Geophys Res Lett 33(22)

Duan AM, Xiao ZX (2015) Does the Climate Warming Hiatus Exist Over the Tibetan Plateau? Sci Rep 5:13711

Duan A, Wu G, Liu Y et al (2012) Weather and climate effects of the Tibetan Plateau. Adv Atmos Sci 29(5):978–992

Fallah B, Cubasch U, Prömmel K et al (2016) A numerical model study on the behaviour of Asian summer monsoon and AMOC due to orographic forcing of Tibetan Plateau. Clim Dyn 47(5):1485–1495

Harrison TM, Copeland P, Kidd WSF, Yin A (1992) Raising Tibet. Science 255:1663–1670

Higgins RW, Yao Y, Wang XL (1997) Influence of the North American monsoon system on the US summer precipitation regime. J Clim 10(10):2600–2622

Hoskins BJ, Karoly DJ (1981) The steady linear response of a spherical atmosphere to thermal and orographic forcing. J Atmos Sci 38:1179–1196

Hu Q, Jiang DB, Fan GZ (2015) Climate change projection on the Tibetan Plateau: Results of CMIP5 models [in Chinese]. Chin J Atmos Sci 39:260–270

Hu S, Cheng J, Chou J (2017) Novel three-pattern decomposition of global atmospheric circulation: generalization of traditional two-dimensional decomposition. Clim Dyn 49(9):3573–3586

Hu S, Chou J, Cheng J (2018) Three-pattern decomposition of global atmospheric circulation: part I—decomposition model and theorems. Clim Dyn 50(7):2355–2368

Huber M, Goldner A (2012) Eocene monsoons. J Asian Earth Sci 44:3–23

Iqbal MJ, Rehman SU, Hameed S et al (2019) Changes in Hadley circulation: the Azores high and winter precipitation over tropical northeast Africa. Theor Appl Climatol 137(3):2941–2948

Jiang D, Ding Z, Drange H et al (2008) Sensitivity of East Asian climate to the progressive uplift and expansion of the Tibetan Plateau under the mid-Pliocene boundary conditions. Adv Atmos Sci 25(5):709–722

Julian PR, Chervin RM (1978) A study of the Southern Oscillation and Walker Circulation phenomenon. Mon Weather Rev 106:1433–1451

Kroon D, Steens T, Troelstra SR (1991) Onset of the monsoonal related upwelling in the western Arabian Sea as revealed by planktonic foraminifera. In: Prell WL et al (eds) Proceedings of the Ocean Drilling Program, Scientific results, Volume 117: College Station, Texas, Ocean Drilling Program, pp 257–263

Kushnir Y, Seager R, Ting M, Naik N, Nakamura J (2010) Mechanisms of tropical Atlantic SST influence on North American precipitation variability. J Clim 23:5610–5628

Lintner BR, Boos WR (2019) Using atmospheric energy transport to quantitatively constrain South Pacific convergence zone shifts during ENSO. J Clim 32(6):1839–1855

Liu X, Yin ZY (2002) Sensitivity of East Asian monsoon climate to the uplift of the Tibetan Plateau. Palaeogeogr Palaeoclimatol Palaeoecol 183(3–4):223–245

Liu B, Zhou T (2017) Atmospheric footprint of the recent warming slowdown. Sci Rep 7(1):1–7

Liu F, Chai J, Wang B et al (2016) Global monsoon precipitation responses to large volcanic eruptions. Sci Rep 6(1):1–11

Lu M, Yang S, Li Z et al (2018) Possible effect of the Tibetan Plateau on the "upstream" climate over west Asia, North Africa, south Europe and the North Atlantic. Clim Dyn 51(4):1485–1498

Mamalakis A, Randerson JT, Yu JY et al (2021) Zonally contrasting shifts of the tropical rain belt in response to climate change. Nat Clim Chang 1–9

Molnar P, Boos W, Battisti D (2010) Orographic controls on climate and paleoclimate of Asia: thermal and mechanical roles for the Tibetan Plateau. Annu Rev Earth Planet Sci 38(1):77–102

Nan SL, Zhao P, Yang S (2009) Springtime tropospheric temperature over the Tibetan Plateau and evolution of the tropical Pacific SST. J Geophys Res 114:D10104

Park HS, Chiang JC, Bordoni S (2012) The mechanical impact of the Tibetan Plateau on the seasonal evolution of the South Asian monsoon. J Clim 25(7):2394–2407

Parsons LA, Yin J, Overpeck JT et al (2014) Influence of the Atlantic Meridional Overturning Circulation on the monsoon rainfall and carbon balance of the American tropics. Geophys Res Lett 41(1):146–151

Pascale S, Bordoni S, Kapnick SB, Vecchi GA et al (2016) The impact of horizontal resolution on North American Monsoon Gulf of California moisture surges in a suite of coupled global climate models. J Clim 29(21):7911–7936

Pascale S, Boos WR, Bordoni S et al (2017) Weakening of the North American monsoon with global warming. Nat Clim Chang 7(11):806–812

Pascale S, Carvalho LMV, Adams DK et al (2019) Current and future variations of the monsoons of the Americas in a warming climate. Curr Clim Chang Rep 5(3):125–144

Prell WL, Kutzbach JE (1992) Sensitivity of the Indian monsoon to forcing parameters and implications for its evolution. Nature 360(6405):647–652

Qiao S, Zou M, Tang S et al (2020) The enhancement of the impact of the wintertime North Atlantic Oscillation on the subsequent sea surface temperature over the tropical Atlantic since the middle 1990s. J Clim 33(22):9653–9672

Quade J, Cerling TE, Bowman JR (1989) Development of Asian monsoon revealed by marked ecological shift during the latest Miocene in northern Pakistan. Nature 342(6246):163–166

Rossby CG (1939) Relation between variations in the intensity of the zonal circulation of the atmosphere and the displacements of the semi-permanent centers of action. J Mar Res 2:38–55

Su B, Jiang D, Zhang R et al (2018) Difference between the North Atlantic and Pacific meridional overturning circulation in response to the uplift of the Tibetan Plateau. Clim past 14(6):751–762

Tang H, Micheels A, Eronen JT et al (2013) Asynchronous responses of East Asian and Indian summer monsoons to mountain uplift shown by regional climate modelling experiments. Clim Dyn 40(5):1531–1549

Trenberth KE, Solomon A (1994) The global heat balance: Heat transports in the atmosphere and ocean. Clim Dyn 10(3):107–134

Varuolo-Clarke AM, Reed KA, Medeiros B (2019) Characterizing the North American monsoon in the community atmosphere model: sensitivity to resolution and topography. J Clim 32(23):8355–8372

Wang B, Ding Q (2008) Global monsoon: dominant mode of annual variation in the tropics. Dyn Atmos Oceans 44(3–4):165–183

Wang B, Bao Q, Hoskins B et al (2008) Tibetan Plateau warming and precipitation changes in East Asia. Geophys Res Lett 35(14)

Wang B, Liu J, Kim HJ et al (2012) Recent change of the global monsoon precipitation (1979–2008). Clim Dyn 39(5):1123–1135

Wang C, Zhang L, Lee SK, Wu L, Mechoso CR (2014) A global perspective on CMIP5 climate model biases. Nat Clim Chang 4:201–205

Wang Z, Yang S, Duan A et al (2019) Tibetan Plateau heating as a driver of monsoon rainfall variability in Pakistan. Clim Dyn 52(9):6121–6130

Wang B, Biasutti M, Byrne MP et al (2021) Monsoons climate change assessment. Bull Am Meteorol Soc 102(1):E1–E19

Webster PJ, Magana VO et al (1998) Monsoons: processes, predictability, and the prospects for prediction. J Geophys Res 103:14451–14510

Wen Q, Yang H (2020) Investigating the role of the Tibetan Plateau in the formation of Pacific meridional overturning circulation. J Clim 33(9):3603–3617

Wen Q, Yao J, Döös K et al (2018) Decoding hosing and heating effects on global temperature and meridional circulations in a warming climate. J Clim 31(23):9605–9623

Wen Q, Döös K, Lu Z et al (2020) Investigating the role of the Tibetan Plateau in ENSO Variability. J Clim 33(11):4835–4852

Wu G, Liu Y, Dong B et al (2012) Revisiting Asian monsoon formation and change associated with Tibetan Plateau forcing: I. Formation. Clim Dyn 39(5):1169–1181

Xie SP, Deser C, Vecchi GA et al (2010) Global warming pattern formation: sea surface temperature and rainfall. J Clim 23(4):966–986

Yang H, Wen Q (2020) Investigating the role of the Tibetan Plateau in the formation of Atlantic meridional overturning circulation. J Clim 33(9):3585–3601

Yang H, Li Q, Wang K et al (2015) Decomposing the meridional heat transport in the climate system. Clim Dyn 44(9–10):2751–2768

Yang H, Wen Q, Yao J et al (2017) Bjerknes compensation in meridional heat transport under freshwater forcing and the role of climate feedback. J Clim 30(14):5167–5185

Yang H, Shen X, Yao J et al (2020) Portraying the impact of the Tibetan Plateau on global climate. J Clim 33(9):3565–3583

Zhang KX, Wang GC, Ji JL et al (2010) Paleogene-Neogene stratigraphic realm and sedimentary sequence of the Qinghai-Tibet Plateau and their response to uplift of the plateau. Sci China Earth Sci 53(9):1271–1294

Zhang RH, Su FG, Jiang ZH, Gao XJ, Guo DL, Ni J, You QL, Lan C, Zhou BT (2015) An overview of projected climate and environmental changes across the Tibetan Plateau in the 21st century [in Chinese]. Chin Sci Bull 60:3036–3047

Zhang W, Zhou T, Zhang L (2017) Wetting and greening Tibetan Plateau in early summer in recent decades. J Geophys Res 122:5808–5822

Zhao P, Zhu Y, Zhang R (2007) An Asian-Pacific teleconnection in summer tropospheric temperature and associated Asian climate variability. Climate Dyn 29:293–303

Zhao P, Yang S, Wu R, Wen Z, Chen J, Wang H (2012) Asian origin of interannual variations of summer climate over the extratropical North Atlantic Ocean. J Clim 25:6594–6609

Terms and Conditions

Springer Nature journal content, brought to you courtesy of Springer Nature Customer Service Center GmbH (“Springer Nature”).
Springer Nature supports a reasonable amount of sharing of research papers by authors, subscribers and authorised users (“Users”), for small-scale personal, non-commercial use provided that all copyright, trade and service marks and other proprietary notices are maintained. By accessing, sharing, receiving or otherwise using the Springer Nature journal content you agree to these terms of use (“Terms”). For these purposes, Springer Nature considers academic use (by researchers and students) to be non-commercial.
These Terms are supplementary and will apply in addition to any applicable website terms and conditions, a relevant site licence or a personal subscription. These Terms will prevail over any conflict or ambiguity with regards to the relevant terms, a site licence or a personal subscription (to the extent of the conflict or ambiguity only). For Creative Commons-licensed articles, the terms of the Creative Commons license used will apply.
We collect and use personal data to provide access to the Springer Nature journal content. We may also use these personal data internally within ResearchGate and Springer Nature and as agreed share it, in an anonymised way, for purposes of tracking, analysis and reporting. We will not otherwise disclose your personal data outside the ResearchGate or the Springer Nature group of companies unless we have your permission as detailed in the Privacy Policy.
While Users may use the Springer Nature journal content for small scale, personal non-commercial use, it is important to note that Users may not:

1. use such content for the purpose of providing other users with access on a regular or large scale basis or as a means to circumvent access control;
2. use such content where to do so would be considered a criminal or statutory offence in any jurisdiction, or gives rise to civil liability, or is otherwise unlawful;
3. falsely or misleadingly imply or suggest endorsement, approval , sponsorship, or association unless explicitly agreed to by Springer Nature in writing;
4. use bots or other automated methods to access the content or redirect messages
5. override any security feature or exclusionary protocol; or
6. share the content in order to create substitute for Springer Nature products or services or a systematic database of Springer Nature journal content.

In line with the restriction against commercial use, Springer Nature does not permit the creation of a product or service that creates revenue, royalties, rent or income from our content or its inclusion as part of a paid for service or for other commercial gain. Springer Nature journal content cannot be used for inter-library loans and librarians may not upload Springer Nature journal content on a large scale into their, or any other, institutional repository.
These terms of use are reviewed regularly and may be amended at any time. Springer Nature is not obligated to publish any information or content on this website and may remove it or features or functionality at our sole discretion, at any time with or without notice. Springer Nature may revoke this licence to you at any time and remove access to any copies of the Springer Nature journal content which have been saved.
To the fullest extent permitted by law, Springer Nature makes no warranties, representations or guarantees to Users, either express or implied with respect to the Springer nature journal content and all parties disclaim and waive any implied warranties or warranties imposed by law, including merchantability or fitness for any particular purpose.
Please note that these rights do not automatically extend to content, data or other material published by Springer Nature that may be licensed from third parties.
If you would like to use or distribute our Springer Nature journal content to a wider audience or on a regular basis or in any other manner not expressly permitted by these Terms, please contact Springer Nature at

onlineservice@springernature.com